Atmos. Chem. Phys. Discuss., 15, 5959–6007, 2015
www.atmos-chem-phys-discuss.net/15/5959/2015/
doi:10.5194/acpd-15-5959-2015

Atmospheric Chemistry and Physics Discussions
Open Access

Brown carbon aerosol in the North American continental troposphere: sources, abundance, and radiative forcing

J. Liu[1,*], E. Scheuer[2], J. Dibb[2], G. S. Diskin[3], L. D. Ziemba[3], K. L. Thornhill[3], B. E. Anderson[3], A. Wisthaler[4], T. Mikoviny[5], J. J. Devi[6], M. Bergin[6], A. E. Perring[7,8], M. Z. Markovic[7,8], J. P. Schwarz[7,8], P. Campuzano-Jost[8,9], D. A. Day[8,9], J. L. Jimenez[8,9], and R. J. Weber[1]

[1]School of Earth and Atmospheric Sciences, Georgia Institute of Technology, Atlanta, GA, USA
[2]Institute for the Study of Earth, Oceans, and Space, University of New Hampshire, Durham, NH, USA
[3]NASA Langley Research Center, Hampton, VA, 23681, USA
[4]Institute of Ion Physics and Applied Physics, University of Innsbruck, Innsbruck, Austria
[5]Oak Ridge Associated Universities (ORAU), Oak Ridge, TN, USA
[6]School of Civil & Environmental Engineering, Georgia Institute of Technology, Atlanta, GA, USA
[7]Chemical Sciences Division, Earth System Research Laboratory, National Oceanic and Atmospheric Administration, Boulder, Colorado, USA

[8]Cooperative Institute for Research in Environmental Sciences, University of Colorado, Boulder, CO, USA
[9]Department of Chemistry and Biochemistry, University of Colorado, Boulder, CO, USA
[*]now at: Atmospheric Sciences and Global Change Division, Pacific Northwest National Laboratory, Richland, WA, USA

Received: 22 January 2015 – Accepted: 5 February 2015 – Published: 3 March 2015

Correspondence to: R. Weber (rodney.weber@eas.gatech.edu)

Published by Copernicus Publications on behalf of the European Geosciences Union.

Abstract

Chemical components of organic aerosol selectively absorb light at short wavelengths. In this study, the prevalence, sources, and optical importance of this so-called brown carbon (BrC) aerosol component are investigated throughout the North American continental tropospheric column during a summer of extensive biomass burning. Spectrophotometric absorption measurements on extracts of bulk aerosol samples collected from an aircraft over the central USA were analyzed to directly quantify BrC abundance. BrC was found to be prevalent throughout the 1 to 12 km altitude measurement range, with dramatic enhancements in biomass burning plumes. BrC to black carbon (BC) ratios, under background tropospheric conditions, increased with altitude, consistent with a corresponding increase in the Absorption Ångström Exponent (AAE) determined from a 3-wavelength Particle Soot Absorption Photometer (PSAP). The sum of inferred BC absorption and measured BrC absorption at 365 nm was within 3 % of the measured PSAP absorption for background conditions and 22 % for biomass burning. A radiative transfer model showed that BrC absorption reduced top of atmosphere aerosol forcing by ~ 20 % in the background troposphere. Extensive radiative model simulations applying this studies background tropospheric conditions provided a look-up chart for determining radiative forcing efficiencies of BrC as a function of surface-measured BrC–BC ratio and single scattering albedo (SSA). The chart is a first attempt to provide a tool for better assessment of brown carbon's forcing effect when one is limited to only surface data. These results indicate that BrC is an important component of direct aerosol radiative forcing.

1 Background

Carbonaceous components of atmospheric aerosols are known to affect climate through direct scattering and absorption of solar radiation. The most prevalent carbonaceous aerosol component is the organic aerosol fraction (OA), which until recently was

ACPD
15, 5959–6007, 2015

assumed to only scatter light and act to cool the climate (Koch et al., 2007; Myhre et al., 2008). The black carbon (BC) fraction efficiently absorbs light and substantially warms the atmosphere (Bond et al., 2013). Globally, BC forcing is ranked the third most important anthropogenic climate-warming agent after carbon dioxide and methane (IPCC, 2013), considering both direct and indirect effects. Recent studies have shown, however, that components of OA also contribute to light absorption (Yang et al., 2009; Zhang et al., 2011, 2013) and that their influence on climate may be substantial (Bahadur et al., 2012; Chung et al., 2012; Feng et al., 2013; Park et al., 2010). These compounds are referred to as Brown Carbon (BrC hereafter) because they tend to absorb light most efficiently at short wavelengths.

A variety of studies have investigated the sources for BrC. Primary BrC is known to be emitted directly from incomplete combustion of fossil or biomass fuels (Hoffer et al., 2006; Lukacs et al., 2007; Andreae and Gelencser, 2006), and secondary organic aerosol (SOA) formed from combustion emissions may also be brown (Saleh et al., 2013; Zhang et al., 2013). Laboratory studies find that light-absorbing secondary compounds (chromophores) can be formed by a variety of mechanisms, including aromatic-SOA production under high levels of nitrogen oxides (NO_x), and through various aqueous phase reactions, such as lignin (Hoffer et al., 2006) and isoprene oxidation (Limbeck et al., 2003). They can also be formed from reactions of carbonyls (e.g., glyoxal, methylglyoxal) in acidic solutions (Sareen et al., 2010), with amino acids (de Haan et al., 2009), methyl amines (de Haan et al., 2009), or ammonium salts (Sareen et al., 2010). Concentrating of solutes during droplet evaporation can also enhance BrC formation (Zarzana et al., 2012). While BrC can be lost by wet and dry deposition, analogous to OA, atmospheric aging of aerosols may also lead to a loss of BrC due to photo-bleaching (Lee et al., 2014; Zhong et al., 2014).

BrC can be difficult to identify with aerosol optical instruments. Lack and Langridge (2013) suggested that the use of an observed wavelength dependence of light absorption, described by the Absorption Ångström Exponents (AAE), to predict BrC absorption leads to substantial uncertainties. Difficulties arise because optical instruments

ACPD
15, 5959–6007, 2015

cannot measure BrC independently of BC. Typically, BrC is determined based on differences between the observed absorption at low wavelengths, where BrC absorption is effective, to what is expected from BC alone. Both factors in the difference calculation are uncertain. However, one of the main uncertainties is related to what BC absorption should be, independent of other absorbers. Some studies indicate that BC mixing state with non-absorbing materials can lead to substantial shifts in AAE relative to pure BC (Lack and Langridge, 2013), making it difficult to attribute enhanced light absorption at low wavelengths to BC mixing state or BrC, if based solely on absorption Ångström exponents.

A more definitive and sensitive approach for identifying BrC is possible by directly measuring chromophores in aerosol solution extracts, since the method can isolate BrC from other absorbers (BC and mineral dust) and long-path absorption cells provide a measurement with high sensitivity. These direct measurements of BrC show that it is ubiquitous. BrC has been shown to be strongly linked to biomass burning and HUmic-Like Substances (HULIS) throughout Europe (Lukacs et al., 2007). In the southeastern US, BrC has been found in rainwater from continental sources (Kieber et al., 2006), while BrC in $PM_{2.5}$ was associated with biomass burning in winter and summer, along with possible contribution from SOA formation (Hecobian et al., 2010; Zhang et al., 2012; Washenfelder et al., 2015).

Chromophores in the ambient aerosol that produce the observed BrC optical properties are not well characterized. Zhang et al. (2013) identified a number of water-soluble nitro-aromatic compounds responsible for BrC in Los Angeles SOA, but they only accounted for $\sim 4\,\%$ of observed BrC absorption at 365 nm. 4-nitrocatechol ($C_6H_5NO_4$) was identified as the largest contributor at roughly 1.4 %. Similar nitro-aromatic chromophores have been identified in fogs (Desyaterik et al., 2013) and aerosols (Mohr et al., 2013) impacted by biomass burning.

Although studies of BrC based on aerosol extracts have been used to investigate the sources, extent and chemistry of fine particulate BrC, it is difficult to use this method to assess optical properties of BrC-containing particles. To estimate optical proper-

ACPD
15, 5959–6007, 2015

ties from solution data, Liu et al. (2013) used size-resolved measurements of aerosol extract light absorbance from several sites to estimate light absorption (b_{ap}) by BrC-containing particles, assuming that the BrC was externally mixed with other absorbers. In this study, we apply these results to aircraft-based filter measurements and use the direct measurements of chromophores in solutions to estimate the extent and sources of BrC throughout the US continental troposphere (up to ~ 12 km altitude). A closure analysis is performed comparing the sum of light absorption at 365 nm from BC and BrC to measurements extrapolated from a 3-wavelength PSAP, averaged over filter sampling intervals, to assess our method for inferring BC and BrC. The importance of BrC is then determined through a radiative transfer model using altitude-resolved BC and BrC data to delineate absorbing aerosol forcing in the continental troposphere from these two components. Since column measurements are rare, the average background tropospheric vertical profile measured in this study is used to create a chart that allows estimation of BrC top of atmosphere (TOA) forcing based on surface measurements of aerosol optical properties and aerosol optical depth.

2 Method

2.1 NASA DC-8 research aircraft measurements during the DC3 campaign

Filters were collected from the NASA DC-8 research aircraft, based out of Salina, KS, between May and June 2012 as part of the Deep Convective Clouds and Chemistry (DC3) campaign (Barth et al., 2014). The study area focused on the central USA and filter samples were obtained from near-surface to an altitude of roughly 12 km a.s.l. (pressure altitude). Figure 1a shows the locations of filter sampling periods during the study, color-coded by altitude.

ACPD
15, 5959–6007, 2015

2.2 Filter sampling, extraction and analysis

The filter sampling system captured particles nominally smaller than 4.1 µm aerodynamic diameter (McNaughton et al., 2007) onto 1 µm pore, 90 mm diameter, Teflon (EMD Millipore) filters. Sampling was generally done during level flight legs with typically 5 min integration times. In total, 609 filter samples were obtained from 22 flights, along with 2 field blanks per flight. Data were corrected by subtraction of the average blank for each flight. Over the course of the study, filters were not uniformly collected over the measurement column. Figure 1b shows the filter sampling frequency (number of filters collected/total filters) as a function of altitude.

Filters were extracted first in 15 ml of high purity water (18.3 MΩ) by 30 min of sonication. The liquid extracts were then filtered via a 25 mm-diameter 0.45 µm pore syringe filter (Fisher Scientific, Fisherbrand* Syringe Filters) to remove insoluble components. Water extracts were transferred into a Liquid Waveguide Capillary Cell coupled to a Total Organic Carbon (LWCC-TOC) analyzer. The combined system quantifies the water-soluble UV-Vis (nominally 200 to 800 nm wavelength range) light absorption spectra (referred to here as, $H_2O\_Abs(\lambda)$) and water-soluble organic carbon (WSOC) mass following the method by Hecobian et al. (2010). (See Table 1 for a list of acronyms). The limit of detection (LOD) was determined as 3 times the SD of field blanks. At 365 nm the LOD of the solution light absorption measurement ($H_2O\_Abs(365)$) was 0.031 $M\,m^{-1}$, whereas the WSOC LOD is estimated at 0.084 $\mu gC\,m^{-3}$. Measurement uncertainties are estimated at 20 % for $H_2O\_Abs(365)$ and 9 % for WSOC, based on uncertainties and variability in water blanks, field blanks, standards, and duplicate measurements.

Following water extraction, the extraction vial and filter were drained and dried by inverting, then the filter was re-extracted in 15 mL of methanol (VWR International, A.C.S. Grade) following the same procedure as the water extract, however in this case only the UV-Vis absorption spectra were measured. The estimated LOD for methanol-soluble light absorption at a wavelength of 365 nm ($MeOH\_Abs(365)$) is 0.11 $M\,m^{-1}$ with an uncertainty of 27 %. Here, total solution absorption due to BrC ($Total\_Abs(\lambda)$) is deter-

ACPD
15, 5959–6007, 2015

mined from the sum of water-soluble and methanol-extracted absorption from the sequential extraction process, under the assumption that this process dissolves all chromophores (Chen and Bond, 2010) (Total_Abs(365) uncertainty is roughly ±34 %). Tests with filters loaded with ambient particles from urban Atlanta show that the methanol extraction, by itself, tends to also include most water-soluble compounds and that the sequential extraction is comparable to methanol extraction alone; the sum of light absorption from extractions of water plus methanol in series were within ∼ 10 % of just methanol extraction (N = 18).

2.3 Online measurements

2.3.1 Gases

A number of gases were used in this study as emissions tracers. Biomass burning was identified using acetonitrile (CH_3CN) and carbon monoxide (CO). Acetonitrile was measured via PTR-MS (uncertainty of ±20 %) and CO by a Diode laser spectrometer (uncertainty of ±2 % or 2 ppbv).

2.3.2 Aerosols

Particle light absorption coefficients (b_{ap}) were measured with a Particle Soot Absorption Photometer (PSAP, Radiance Research) at wavelengths of 470, 532, and 660 nm. The inlet had an intrinsic 50 % cut size of 4.1 µm, consistent with the filter collection, and the sample air was dried (RH typically less than 40 %). As a filter-based optical instrument, where particle absorption is determined from light attenuation through a filter being loaded with particles, the PSAP suffers from various artifacts (Bond et al., 1999; Petzold et al., 2005). This includes multiple scattering by the filter fibers and by aerosols embedded on or within the filter; the latter increases with filter loading. Reported PSAP b_{ap} data were adjusted using Virkkula et al. (2010). Based on the operation of the instrument, the PSAP absorption coefficients are estimated to have an uncertainty of

ACPD
15, 5959–6007, 2015

20 % or 0.2 $\mathrm{M\,m^{-1}}$, whichever is larger. Artifacts that depend on aerosol composition, however, may increase this uncertainty (Lack et al., 2008). All PSAP data used in the following analyses have been averaged to filter sampling times.

Refractory black carbon (rBC, here referred to just as BC to minimize confusion with BrC) mass concentrations were measured with a SP2 (Single Particle Soot Photometer) and corrected to account for accumulation-mode BC at sizes outside the detection range of the instrument (Schwarz et al., 2008). The instrument was calibrated with fullerene soot (Alfa Aesar Lot #F12S011), the accepted calibration material for the instrument (Baumgardner et al., 2012). Estimated uncertainty is 30 % from flow and BC mass calibrations and aspiration efficiency. OA was measured with a high resolution time-of-flight Aerodyne Aerosol Mass Spectrometer (AMS) (DeCarlo et al., 2006) with an estimated uncertainty of 38 %. In the following analysis, online data were averaged to filter sampling times and included in the analysis if the online data covered greater than 75 % of the sampling time. All aircraft data are blank corrected and reported at standard temperature and pressure (273 K and 1013 mb).

The ambient light scattering coefficients (b_{sp}), used in the subsequent radiative transfer model, were measured by a TSI Integrating nephelometer at wavelengths of 450, 550, and 700 nm. The inlet cut-point was the same as other instruments (aerodynamic diameter of 4.1 µm). Scattering coefficients at three wavelengths were first averaged over the filter-sampling period, if more than 75 % of the period was covered by measurements. The averaged scattering coefficients were then extended to other wavelengths based on a scattering Ångström exponent (SAE) by Eqs. (1) and (2).

$$\mathrm{SAE} = -\frac{\ln\left(b_{sp}(700)\right) - \ln\left(b_{sp}(450)\right)}{\ln(700) - \ln(450)} \tag{1}$$

$$b_{sp}(\lambda) = b_{sp}(550)\cdot\left(\frac{\lambda}{550}\right)^{-\mathrm{SAE}} \tag{2}$$

Excluding biomass burning plumes, the study mean ± SD SAE was 1.27 ± 0.74, Scattering data were reported to have a 10 % uncertainty for measurements at all three

ACPD
15, 5959–6007, 2015

wavelengths, therefore the combined uncertainty in estimated scattering coefficients at various wavelengths, based on Eqs. (1) and (2), was estimated at roughly 20 %.

3 Results

In the following analysis, we first use data on light absorption of the aerosol extracts to investigate sources and distributions of BrC. Following this, the solution data are converted to estimates of BrC aerosol absorption coefficients and the optical effects of BrC are investigated.

3.1 Identifying biomass burning plumes

During the DC3 campaign, 2 out of 22 aircraft flights were specifically targeted to investigate biomass burning emissions, and in six other flights at least one biomass burning plume was encountered. For this work, the data are simply delineated between clearly evident biomass burning sampling periods and all else, the latter being referred to as background tropospheric conditions. To identify biomass burning plumes, CO and CH_3CN were used as tracers following the method of de Gouw et al. (2004). First, enhancements in CO in time-series plots were identified. For these episodes, if r^2 values for CO and CH_3CN were higher than 0.5, the plume was designated as biomass burning. Identified biomass burning sampling periods are listed in Table 2. If greater than 75 % of the filter sampling integration time was identified as a biomass burning plume, it was characterized as biomass burning. By this criterion roughly 12 % of collected filters were identified as biomass burning. Filters not identified are referred to as background measurements, but may still have been influenced, to some extent, by biomass burning due to small-duration plume intercepts. Residual impacts from dispersed biomass burning emissions may also account for some fraction of the ambient aerosol throughout the troposphere during this study. However, the majority of filters

ACPD
15, 5959–6007, 2015

were collected under what could be considered more typical continental tropospheric conditions, albeit during a summer of extensive burning.

3.2 Study statistical summary

A summary of the DC3 BrC solution measurements, together with other relevant species, is given in Table 3. BrC in filter extracts was observed throughout the study region, with over 85 % of the data above the LOD.

Comparing with background conditions, biomass burning plumes were notable by significantly higher BrC levels. Average H_2O_Abs(365) in the identified biomass burning plumes were 5 times higher than background conditions, while Total_Abs(365) was approximately 4 times higher. In contrast, the enhancement in other species were smaller; WSOC was only ~ 1.3, OA 2.8 and BC 2.6 times higher than background conditions. The differential enhancement of WSOC and H_2O_Abs(365) or Total_Abs(365) indicates that biomass burning aerosol is browner on a per mass basis (higher mass absorption efficiencies) than the background aerosol, as seen in other studies (Hecobian et al., 2010). These results confirm that biomass burning is a strong source for both water- and methanol-soluble BrC and are consistent with studies using different methods to identify BrC and biomass burning (Lack et al., 2013).

The proportion of water to methanol soluble BrC was different in background vs. biomass burning plumes. In background air masses, the water-soluble BrC fraction was roughly 25 to 33 % (i.e., H_2O_Abs(365)/Total_Abs(365)), similar to previous studies (Zhang et al., 2013; Liu et al., 2013). However, the water-soluble BrC fraction was higher in biomass burning plumes, where H_2O_Abs(365) comprised ~ 45 % of the Total_Abs(365). These data suggest that primary smoke emissions contain or form more water relative to methanol-soluble BrC compared to aged BrC.

ACPD
15, 5959–6007, 2015

3.3 Correlations

Associations between various species in both the biomass burning plumes and under background conditions are investigated based on correlations. Results are summarized in Table 4. Correlations are shown for H_2O_Abs(365) and Total_Abs(365). Since, for background conditions, two thirds to three quarters of the BrC absorption is associated with the methanol extract, Total_Abs(365) correlations with various other species are driven primarily by the methanol-soluble BrC (for brevity, we do not show correlations for just the methanol-soluble BrC). Note that for airborne measurements, temporal correlations imply spatial correlations between species.

For biomass burning samples, species expected from the smoke plumes (e.g., CO, acetonitrile, OA, WSOC, BC and PSAP b_{ap} at all three wavelengths) are highly correlated with each other, and all are highly correlated with both H_2O_Abs(365) and Total_Abs(365), consistent with a common source. The least correlated were WSOC and BC ($r = 0.7$), and H_2O_Abs(365) and BC ($r = 0.72$), possibly because some fraction of the water-soluble compounds may be secondary and not as likely to be correlated with a primary component (BC).

In contrast, for background conditions there was a poor correlation between H_2O_Abs(365) and Total_Abs(365) ($r = 0.32$) and they were correlated with a different set of species. H_2O_Abs(365) was correlated mostly with the PSAP measurements of absorption ($r = 0.66$ at 470 nm) or with BC ($r = 0.64$), but not well correlated with WSOC ($r = 0.34$). But, H_2O_Abs(365) was somewhat correlated with OA ($r = 0.57$) and acetonitrile ($r = 0.57$), suggesting that the water-soluble faction in the background troposphere could be more strongly related to primary emissions and possibly linked to aged biomass burning.

Total_Abs(365) was not well correlated with any of the other parameters in the background samples. This lack of correlation suggests that much of the background tropospheric BrC had undergone some form of processing or evolution (e.g., photobleaching). A similar situation is observed for WSOC, which was also not generally correlated

ACPD
15, 5959–6007, 2015

with any of the other variables in Table 4. In a ground-based study, Liu et al. (2013) observed higher relative levels of water to methanol-soluble BrC near sources compared to aged aerosol, consistent with an aging process that produces a higher insoluble BrC fraction.

3.4 Altitude profiles of light absorbing aerosols

These data show that BrC is detected throughout the continental troposphere. Vertical profiles of H_2O_Abs(365) and Total_Abs(365) are given in Fig. 2a and b for both the biomass burning plumes and background conditions. The profiles were constructed by sorting the two data sets into 1 km bins and plotting the bin median. Error bars represent the inter quartile ranges for each bin and demonstrate the large variability in the data, especially for the biomass burning plumes.

BC concentration and PSAP b_{ap} at 660 nm are also plotted. BrC, BC and PSAP absorption show large differences between biomass burning events and background conditions, with the biomass burning plumes dominant at a few altitudes where the aircraft encountered and pursued specific plumes. The biomass burning altitude profiles for BrC, BC and PSAP absorption are all somewhat similar, indicating that biomass burning contributes to all carbonaceous aerosol components that absorb light, as previously shown by the high correlations amongst these species. This is less true for background conditions where differences between the light absorbing components can be seen, for example, BC concentrations are generally more elevated closer to the surface.

To compare vertical distributions of aerosol light absorbing components in background air masses, the cumulative column fraction of light absorption coefficient or BC concentration is plotted in Fig. 3. At a given altitude, the cumulative fraction is the light absorption coefficient, or concentration, integrated over all altitudes above, relative to the total column. Note that the integral of the actual absorption occurring would depend on the vertical profile of actinic flux; this is independent of the relative distributions that we explore here. Half the column BC concentration occurs at approximately

ACPD
15, 5959–6007, 2015

3.5 km a.s.l., while for water or total (water plus methanol extract) BrC, this occurs between 5 and 6 km, indicating a more uniform vertical distribution and not as dominated by surface emissions compared to BC. PSAP-determined aerosol absorption at 660 nm and light absorption extrapolated to 365 nm is also shown (the method for extrapolating is discussed below, see Eq. 7). For PSAP absorption efficiency at 365 nm, the 50 % altitude is 4.5 km a.s.l., which is between BC and BrC, suggesting contributions to light absorption by a mixture of BC and BrC at 365 nm, while the 50 % altitude for PSAP absorption efficiency at 660 nm is ~ 4 km a.s.l., closer to BC, as expected, since at 660 nm BC should dominate the total light absorption (i.e., BrC does not effectively absorb at high wavelengths, see next section).

The ratio of BrC (Total_Abs(365)) to the SP2-measured BC mass also increases with altitude, (see Supplemental Fig. S1), further demonstrating the differences in vertical distributions of BrC and BC for the background troposphere. These results suggest there is in-situ BrC production or possibly preferential loss of BC with increasing altitude. Higher BC at the surface may reflect greater contributions from fossil fuel combustion sources for BC. Vertical profiles of aerosols greatly affects overall radiative forcing.

3.5 Absorption Ångström Exponents for BrC and light absorbing aerosols

The wavelength (λ) dependence of light absorption is often fit with a power law of the form:

$$\mathrm{Abs}(\lambda) = K \cdot \lambda^{-\mathrm{AAE}} \tag{3}$$

Where Abs(λ) is the light absorption at a given wavelength (λ) for light passing through a region of light absorbing species (example, the waveguide with liquid extracts, or an aerosol layer in the ambient atmosphere), and AAE is the Absorption Ångström Exponent, (the factor K is not important in this analysis). For the high spectral resolution data available with spectrophotometric measurements of absorption in the water

ACPD
15, 5959–6007, 2015

or methanol aerosol extracts, the AAE (in this case AAE for BrC, AAE_{BrC}) is determined from a linear regression fit of log(Abs(λ)) vs. log(λ) between 300 and 450 nm. Examples of the solution light absorption spectra for a biomass burning sample and typical background sample are shown in Fig. 4, along with the regression fit to determine an AAE_{BrC}. Above roughly 450 nm, in both background and biomass burning plumes, the BrC absorption levels out or increases, which may be due the chemical nature of the chromophores. This range is excluded from the AAE_{BrC} calculation. In the following analysis AAEs for ambient aerosols are assumed to be the same as the solution-measured BrC AAE (Moosmuller et al., 2011; Liu et al., 2013).

The BrC absorption Ångstöm exponents were somewhat similar for background conditions and biomass burning samples, however, there were significant differences between water and methanol extracts. For water extracts the mean ± SD of AAE_{BrC} was 6.82 ± 2.63 for background conditions and 8.95 ± 1.73 for biomass burning. Methanol extract AAE_{BrC} was on average 4.54 ± 3.07 for background conditions and 5.04 ± 2.61 for biomass burning plumes. Lower AAE_{BrC} for methanol vs. water extracts (also see Fig. 4) may be related to differences in solubility of the chromophores (Zhang et al., 2013; Chen and Bond, 2010). BrC chemical speciation by Zhang et al. (2013) found that larger molecular weight PAHs absorbed more toward the visible range (i.e., have a lower AAE) and have a lower water-solubility. Methanol extract lower AAE_{BrC} could result from higher molecular weight chromophores not soluble in water.

The AAE for the overall light absorbing ambient aerosol can also be calculated from the more limited spectral data (three wavelengths) associated with the PSAP. Here, AAE_{PSAP} is calculated using absorption measured at the wavelength pair, 470 and 660 nm by;

$$AAE_{PSAP} = -\frac{\ln\left(b_{ap,PSAP}(660)\right) - \ln\left(b_{ap,PSAP}(470)\right)}{\ln(660) - \ln(470)} \quad (4)$$

AAE altitude profiles are plotted in Fig. 5. On average, there is no significant variability in the vertical profiles of background air-mass mean AAE_{BrC}, for either water or

ACPD
15, 5959–6007, 2015

methanol extracts (Fig. 5a). There is however, much more variability within each altitude layer. The cause of this variability could be due to aerosol chemistry, but investigating it is beyond the scope of this analysis.

AAE_{BrC} considers only BrC absorbers, whereas AAE_{PSAP} includes all absorbers (BrC and BC). Average AAE_{PSAP} for the biomass burning periods was 2.15 ± 0.88 (mean ± SD) and 1.60 ± 0.61 for background conditions. Differences can also be seen in the vertical profiles (Fig. 5b), where for the most part, the AAE_{PSAP} was higher in the biomass burning plumes compared to background conditions. Qualitatively, the higher AAE_{PSAP} for the biomass burning air masses is consistent with significant contributions from BrC, although light absorption enhancements due to mixing state cannot be ruled out. Another noteworthy feature of Fig. 5b is that a trend in AAE_{PSAP} may also be evident in the vertical profile for background conditions, where AAE_{PSAP} tends to increase with altitude. This is consistent with the greater fraction of BrC to BC with altitude. Note, that for both biomass burning and background air masses the AAE_{PSAP} is closer to 1 near the surface where BC appears to be more dominant. Overall, the independent measurements of BrC and aerosol AAEs are consistent and suggest that the observed AAEs greater than one are mostly due to BrC and not enhancements due to BC mixing state.

3.6 Light absorption calculations for comparing BrC to BC and PSAP data

In the previous analysis, BrC solution light absorption data was presented. Now, BrC solution data is converted to optical absorption to quantify the separate contributions of BrC and BC as a function of altitude. The sum of BC and BrC absorption are then compared to the PSAP data (total BrC and BC). The analysis could be done at any wavelength, however, 365 nm is chosen since it is in a wavelength range where a reliable BrC measurement is possible, e.g., at lower wavelengths, other non-BrC species begin to impact the data, such as nitrate, but sufficiently low that BrC, if present, should have a significant optical effect (i.e., BrC absorption drops off rapidly with increasing wavelength, as seen above, Fig. 4).

ACPD
15, 5959–6007, 2015

3.6.1 BrC light absorption

To convert the solution absorbance to light absorption by an aerosol, knowledge of both particle morphology and how the chromophores are distributed amongst particle size is needed. In the past, studies have often assumed a small particle limit when making this conversion, where light absorption by BrC aerosol is taken as 0.69 to 0.75 times the light absorption of the solution (e.g., Sun et al., 2007). This likely gives a lower limit for BrC absorption since BrC is not associated with sub-nm size particles. Liu et al. (2013) measured the size distribution of BrC and showed that the chromophores were consistently found in the accumulation mode in both fresh vehicle emissions and for more aged background aerosols (BrC geometric mass mean diameter was $\sim 0.5\,\mu m$). It is likely that this is more representative of the BrC size distribution of the background troposphere, given that the aerosols are aged. This assumption is supported by the AMS size-resolved OA data. OA was predominantly in the accumulation mode throughout the atmospheric column, excluding biomass burning plumes. For background conditions OA geometric mass mean diameters were $0.38 \pm 0.02\,\mu m$ for the altitude range 0–5 km, and $0.37 \pm 0.08\,\mu m$ for 5 km and above.

From Mie theory calculations, assuming that the BrC was externally mixed with other absorbers, Liu et al. (2013) found that aerosol absorption is approximately 1.8 to 2 times higher than the bulk absorption measured in the extracts. Washenfelder et al. (2015) used bulk measurements of BrC absorption at 365 nm to estimate the OA refractive index and used OA size distributions and Mie theory and also found a conversion factor of two for aerosols at a rural site. Thus the aerosol BrC absorption at 365 nm is estimated for the two solvent extracts simply as,

$$b_{ap,H_2O\_BrC}(365) = 2 \cdot H_2O\_Abs(365) \quad (5)$$

$$b_{ap,Total\_BrC}(365) = 2 \cdot [H_2O\_Abs(365) + MeOH\_Abs(365)] = 2 \cdot Total\_Abs(365) \quad (6)$$

ACPD
15, 5959–6007, 2015

Considering the known uncertainty in the conversion factor of 2 (estimated to be at least 30 % (Liu et al., 2013)) and the liquid absorption measurements, the overall uncertainty of these coefficients is estimated to be at least 30 and 45 %.

3.6.2 BC and PSAP light absorption

To estimate light absorption by the ambient aerosol at 365 nm, PSAP measurements at higher wavelengths are extrapolated to 365 nm using a calculated AAE_{PSAP}. Particle absorption at a certain wavelength, $b_{ap,PSAP}(\lambda)$, is calculated from the AAE_{PSAP} from Eq. (3) and the light absorption measured at 660 nm

$$b_{ap,PSAP}(\lambda) = b_{ap,PSAP}(660) \cdot \left(\frac{\lambda}{660}\right)^{-AAE_{PSAP}} \tag{7}$$

It is noted that AAE_{PSAP}, given in Eq. (4), could have been determined from different wavelength combinations (i.e., 470–532, 532–660 nm). For this data set, the other wavelength pairs led to a predicted $b_{ap,PSAP}(365)$ systematically different by roughly 20 % of that predicted by Eqs. (4) and (7). The wavelength pair of 470 and 532 results in a $b_{ap,PSAP}(365)$ that was ~ 20 % higher (regression slope = 1.19, $r^2 = 0.98$, intercept = −0.02 for $b_{ap,PSAP}(365)$ predicted from 470–532 vs. $b_{ap,PSAP}(365)$ predicted from 470–660 wavelength pair). Whereas the other combination produces a systematically 20 % lower $b_{ap,PSAP}(365)$ (regression slope = 0.80, $r^2 = 0.94$, intercept = 0.04 for $b_{ap,PSAP}(365)$ from 532–660 vs. $b_{ap,PSAP}(365)$ predicted from 470–660 wavelength pair). Thus, the 470–660 pair gives the middle value between what is predicted by other possible combinations (see Liu et al. (2014) for how the choice of wavelength pair influences the vertical distribution of AAE_{PSAP}).

Since data on light absorption by BC is not available, it was estimated. A number of possible methods are available. In the first case, BC absorption at a certain wavelength ($b_{ap,BC1}(\lambda)$) is calculated from light absorption coefficients recorded at high wavelengths, where contributions from BrC should be minimal, and extrapolated to

ACPD
15, 5959–6007, 2015

lower wavelengths using an assumed BC AAE (AAE_{BC}),

$$b_{ap,BC1}(\lambda) = b_{ap,PSAP}(660) \cdot \left(\frac{\lambda}{660}\right)^{-AAE_{BC}} \quad (8)$$

Aged BC aerosol is likely to be internally mixed with other aerosol components, which, based on simplified models, such as spherical clear shells over absorbing BC cores (Bond et al., 2006), and limited laboratory data (Schnaiter et al., 2005; Slowik et al., 2007), could lead to a significantly different AAE_{BC}, for example, ranging from 0.86 to 1.6 (Kirchstetter and Thatcher, 2012; Feng et al., 2013; Lack and Cappa, 2010). More random mixtures, or mixtures containing absorbing material, such as BrC, can significantly reduce this enhancement (Lack and Cappa, 2010). Recent ambient data do not show enhancements (Cappa et al., 2012). In the following analysis, an AAE_{BC} of 1 is used as the default case.

Instruments that measure light absorption based on particles deposited on a filter, such as the PSAP, can also be significantly biased high due to artifacts (Lack et al., 2008). To avoid this, an alternative approach to calculate BC absorption is to estimate the light absorption coefficient at high wavelengths, where BrC does not absorb light, using the BC mass concentration and an assumed characteristic BC mass absorption cross-section (MAC) at a given wavelength. BC absorption at other wavelengths can be determined using the AAE_{BC}. Bond and Bergstrom (2006) have suggested a $MAC_{BC} = 7.5 \pm 1.2\,m^2\,g^{-1}$ at 550 nm for pure uncoated (i.e., fresh) BC. Here, we use this as a possible lower bound for BC light absorption and refer to this second method of calculating the BC absorption with a subscript 2,

$$b_{ap,BC2}(\lambda) = MAC_{BC} \cdot BC \cdot \left(\frac{\lambda}{550}\right)^{-AAE_{BC}} \quad (9)$$

For consistency, this prediction of BC absorption is compared to the ambient aerosol absorption (b_{ap2}), which is estimated by extrapolating from this MAC-determined light

ACPD
15, 5959–6007, 2015

absorption coefficient ($b_{ap,BC2}$) using the PSAP AAE,

$$b_{ap2}(\lambda) = b_{ap,BC2}(\lambda) \cdot \left(\frac{660}{\lambda}\right)^{-AAE_{BC}} \cdot \left(\frac{\lambda}{660}\right)^{-AAE_{PSAP}} \quad (10)$$

A schematic showing the various optical calculations is given in Fig. 6.

In this data set, the second approach leads to a lower prediction of BC absorption compared to the first method (i.e., $b_{ap,BC2} < b_{ap,BC1}$, see Fig. 6) due to differences between the assumed MAC_{BC} and the PSAP-measured MAC. For this data set, the non-biomass burning study-average MAC at 660 nm is 10.9 $m^2 g^{-1}$ (see Supplement Fig. S2). This is roughly 75 % higher than the assumed pure BC MAC_{BC}, where MAC_{BC} at 550 nm was converted to a MAC_{BC} at 660 nm, by assuming an AAE_{BC} of 1, resulting in MAC_{BC} at 660 nm = 6.3 $m^2 g^{-1}$. Observed MACs are often found to vary substantially (Chan et al., 2011), and some of this variability is thought to be due to internal mixing of BC. (see Bond et al. (2013) for a review). In summarizing observations of ambient aerosol BC MACs, Bond et al. (2013), suggests that a MAC_{BC} 50 % greater than that of pure BC is reasonable (Bond et al., 2013), which is not significantly different from what we observed. This suggests that the PSAP data for background conditions may not be highly skewed by artifacts.

The schematic in Fig. 6 suggests that light absorption by the ambient aerosol at 365 nm (e.g., $b_{ap,PSAP}(365)$) is higher than that predicted at the same wavelength for BC (e.g., $b_{ap,BC1}(365)$). This is often interpreted to be due to additional absorption by BrC (Kirchstetter et al., 2004; Sandradewi et al., 2008; Chen and Bond, 2010; Sun et al., 2007; Clarke et al., 2007) and is due to the ambient AAE (AAE_{PSAP}) being greater than AAE_{BC} (i.e., 1). However, as noted above, due to uncertainties associated with these various calculations, such as possible variability in AAE_{BC}, definitively attributing the difference to be due to BrC is highly uncertain. However, in this case we have a direct measurement of BrC and an optical closure analysis can be performed to assess if BrC is a reasonable explanation for the difference.

ACPD
15, 5959–6007, 2015

3.7 Optical importance of BrC relative to BC and a closure assessment by comparison to PSAP

In the following we focus on BC absorption based on the PSAP measurements and an assumed AAE_{BC} of 1 (i.e., $b_{ap,BC1}$). Results using the other measure of BC absorption ($b_{ap,BC2}$) are discussed, but not plotted.

3.7.1 Background conditions

Vertical profiles of altitude-binned median data of the light absorption coefficients at 365 nm for BC ($b_{ap,BC1}$), plus either water soluble BrC (b_{ap,H_2O_BrC}) (Fig. 7a), or total BrC ($b_{ap,Total\_BrC}$), are shown in Fig. 7, along with the PSAP data extrapolated to 365 nm ($b_{ap,PSAP}$) representing the ambient light absorption coefficient. Figure 7 shows that absorption drops off with increasing altitude. It is also evident that the absorption of just black carbon ($b_{ap,BC1}$) is always significantly less than the overall ambient aerosol absorption determined from the PSAP, at 365 nm ($b_{ap,PSAP}$). Water-soluble brown carbon absorption, $b_{ap,H_2O\_BrC}(365)$, is small relative to BC and the sum of the two is always lower than the observed absorption ($b_{ap,PSAP}$), which is reasonable as the water-soluble fraction is only a portion of the light-absorbing organics. Total BrC absorption, $b_{ap,Total\_BrC}(365)$, on the other hand, is more comparable to BC absorption over most of the altitude range, and when the two are summed, the BC + BrC tends to agree with the observed absorption. (Note, measurement uncertainties are roughly 28 to 45 % for the various light absorption coefficients).

A more quantitative assessment of closure for background conditions can be seen in a scatter plot with orthogonal distance regression of the sum of the estimated BC and BrC vs. PSAP absorption (Fig. 8). From Fig. 8a, on average for background tropospheric conditions, at 365 nm BC accounts for roughly 74 % of the ambient absorption. When the water-soluble BrC is added, a slope of 0.90 (Fig. 8b) indicates that the BC plus water-soluble BrC improves the closure, but still slightly under-predicts the light absorption coefficient. When the total BrC is used (water + methanol extractions) the

ACPD
15, 5959–6007, 2015

sum of BC and BrC results in a slope near 1 (0.97), but with a positive intercept at 0.56 Mm^{-1}. If the regression is forced through zero, the slope is 1.16. If the low particle limit is used in the conversion of solvent extracts absorption to ambient particle absorption (instead of the factor of 2 (Liu et al. 2013)), the slope would be 0.76 for BC + water-soluble BrC, and 0.85 for BC + total BrC vs. ambient. These comparisons have assumed an AAE_{BC} of 1, but a range of values are possible (i.e., Gyawali et al., 2009). In this case, an AAE_{BC} value of 0.82 would result in regression slope of 1 between the sum of BC and BrC absorption vs. $b_{ap,PSAP}$ at 365 nm, for a solution conversion factor of 2. One cannot definitively attribute all enhanced light absorption at low wavelengths to BrC; some combination of enhancement due to BC mixing and BrC is possible. In this data set, however, an enhancement in light absorption at low wavelengths is most consistent with just BrC.

Finally, in the previous sections we showed the prevalence of BrC increases relative to BC with increasing altitude, based on solution data. Now that the closure analysis provides some support for the BrC absorption coefficients at 365 nm, the fractional contribution of brown carbon absorption (both water and total BrC) relative to ambient absorption can be assessed as a function of altitude. Figure 7c shows that the fraction of BrC substantially increases with increasing altitude, with absorption due to total BrC (at 365 nm) accounting for > 80 % of total absorption above ~ 7.5 km, a region where ambient absorption coefficients are low.

3.7.2 Biomass burning events

Applying a vertical distribution analysis is not possible for biomass burning plumes, since there were limited data points for some of the altitudes, but closure analysis based on the combined data is shown in Fig. 9. The conversion factor from solution BrC to ambient aerosol absorption has not been studied for biomass burning events (Liu et al., (2013) did not include a size-resolved measure of biomass burning BrC), leading to some uncertainty in this closure analysis. As before a multiplication factor of 2 is used as the base case, recognizing there is uncertainty in this assumption.

ACPD
15, 5959–6007, 2015

Biomass burning is known to be a strong source for BrC, and Fig. 9a shows that on average, at 365 nm BC only accounted for roughly 57 % of the light absorption, substantially lower than that for background conditions. For BC plus water-soluble BrC the slope is 77 % and, for BC plus total BrC the slope is 122 %, in this case over-predicting the observed values. An AAE_{BC} value of 0.82, which resulted in slope of 1 for background conditions, results in a smaller (9 %) over-estimation for the biomass burning plumes. More studies of individual biomass burning plumes would provide greater insight into possible roles of both BC mixing and BrC in light absorption enhancements.

3.7.3 Use of the MAC in closure calculations for background conditions

A similar analysis, but where BC and ambient light absorption are based on an assumed BC MAC, SP2-measured BC concentrations, and PSAP AAE (i.e., see Fig. 6, $b_{ap,BC2}$ and b_{ap2})), can also be performed. As discussed in a previous section, this approach leads to a lower prediction of BC absorption compared to the first method (i.e., $b_{ap,BC2} < b_{ap,BC1}$), and therefore a lower b_{ap2} than $b_{ap,PSAP}$ at 365 nm (Fig. 6). In this case the closure analysis for BC vs. ambient light absorption (b_{ap2}) results in a slope of 0.73, whereas BC + water-soluble BrC the slope is 0.97 and for total BrC the slope is 1.40. Thus, unlike when the PSAP absorption coefficients at 660 nm are used directly, the sum of BC and BrC light absorption generally exceeds the ambient total absorption. This happens because using a MAC of pure BC results in substantially lower absorption coefficients, making the proportion of BrC higher. It appears that the use of the MAC_{BC} (7.5 at 550 nm or 6.3 $m^2 g^{-1}$ at 660 nm) in this case does not produce as reasonable a result as absorption coefficients based on the PSAP data (observed study MAC of 10.9 $m^2 g^{-1}$ at 660 nm) and so this method is not considered in the radiative forcing calculations that follow.

ACPD
15, 5959–6007, 2015

3.8 Radiative forcing

The Santa Barbara DISORT Atmospheric Radiative Transfer (SBDART) model was used to assess the role of BrC in direct radiative forcing for background conditions in the continental troposphere. Vertically resolved optical properties were used, including light absorption coefficients for BC, BrC and total absorption based on the PSAP, along with measurements of the light scattering coefficients from the multi wavelength nephelometer. Absorption and scattering coefficients were calculated for 10 wavelengths, over the 300–700 nm range, and average values were determined for each 1 km altitude bin. BC absorption was determined using Eq. (8) and $AAE_{BC} = 1$, BrC was based on the AAEs from the total (water + methanol) solution data, and overall ambient aerosol light absorption was based on Eq. (7) and inferred AAE_{PSAP}. Scattering coefficients were determined from Eq. (2). The scattering is based on measurements and independent of the light absorption used (i.e., just BC or BC plus BrC). The wavelength-dependent single scattering albedo (SSA) was then calculated as input to the SBDART model. Aerosol optical depth (AOD) was also calculated using absorption and scattering data. The SBDART model interpolated from these data over the wavelength range of 250 to 4000 nm. A third input needed for SBDART is the asymmetry parameter (g), of which a uniform value of 0.65 (Carrico et al., 2003) was used across all wavelengths. An atmospheric profile for a standard mid-latitude summer was assumed and tested with albedo resulting from surface types of both sand and vegetation. The model was run with solar zenith angle (SZA) ranging from 0–85 degrees, at 5° increments. Daily average forcing is the integrated instantaneous radiative forcing averaged over a 24 h period.

To assess the influence of BrC relative to BC, forcing was calculated based on the estimates of BC optical properties ($AAE_{BC} = 1$), then compared to forcing for BC + BrC. Four groups of wavelength-dependent inputs were generated for each altitude bin; no aerosol (gases only), scattering aerosols only, BC as the only absorbing aerosol, and BC + BrC as absorbing aerosols. Only background data were used (i.e., biomass

ACPD
15, 5959–6007, 2015

burning plumes were excluded), to better represent typical continental atmospheric conditions. At a SZA of 40°, considering all aerosol direct optical effects, but delineating absorption by BC and BrC, the instantaneous forcings at top of atmosphere (TOA) were −19.33 and −24.84 $W m^{-2}$ for BC + BrC and BC, respectively, with vegetation as surface type, and −23.35 and −28.57 $W m^{-2}$ for a surface of sand. Integrated over 24 h period, diurnally averaged forcings at TOA were −14.79 and −11.82 $W m^{-2}$ for BC and BC + BrC, vegetation surface type, and −16.94 and −14.11 $W m^{-2}$, respectively, for a surface type of sand. The overall negative TOA forcing is due to cooling by aerosol scattering; however, BrC absorption appreciably changes the TOA forcing relative to BC only, resulting in roughly 20 % less cooling compared to only BC. The forcings at the surface are discussed in Liu et al. (2014).

Alternatively, we could use the PSAP data to estimate total light absorption by aerosols instead of BC + BrC, in which case we get light absorbers other than BC (eg, BrC, dust) contributing ∼ 17 %, similar to the values reported above. Other combinations of the analyses are possible, but all give similar results. Therefore, for the aerosol loadings recorded in this study, we find that BrC increased the shortwave solar absorption in the atmosphere by approximately 20 %, demonstrating the importance of BrC as a climate forcing agent.

Most measurements of BrC and other aerosol optical properties are made at the surface. To allow estimates of TOA forcing due to contributions of aerosol BrC throughout the column, the average distributions of single scattering albedo and optical depth observed under background conditions is used to generate a chart relating aerosol radiative forcing efficiencies (RF_{eff}) as a function of the aerosol absorption coefficient of BrC relative to BC at 365 nm and SSA measured at the surface. The RF_{eff} is defined as the TOA aerosol radiative forcing divided by aerosol optical depth (AOD) at 500 nm. Figure 10 was generated through multiple runs (N = 4320) of SBDART and shows that RF_{eff} values of BrC increases with decreasing SSA and increasing BrC/BC ratio, as both factors result in higher BrC at a given AOD. The circle in the figure represents the average background conditions during this campaign, with a value of 16.71 $W m^{-2}$ per

ACPD
15, 5959–6007, 2015

unit optical depth at 500 nm, with a surface of vegetation. In comparison, the forcing efficiency is $-88.64\,\mathrm{W\,m^{-2}}$ per unit optical depth at 500 nm for BC + scattering, which is in agreement with previous research (e.g., Bush and Valero, 2003).

If the vertical profiles applied in SBDART represents typical background tropospheric conditions in the continental US, application of Fig. 10 is not limited to this campaign. Further airborne studies similar to this one are needed to assess this assumption. As noted, the SSA and BrC/BC absorption ratios plotted in the figure are surface values at 365 nm, while column AOD could be easily retrieved from satellite data, for example, AOD at 500 nm is available from AERONET. Therefore, the figure can serve as a look-up chart to estimate radiative forcing contributions by BrC, when altitude-resolved parameters are not available. For example, a data point for surface measurements at a rural site in the southeastern US (Washenfelder et al., 2015) is also shown in Fig. 10. In addition, large-scale models require substantial number of computations, the patterns shown in this figure could be considered as a simplified module and incorporated into models with minimal computational costs.

4 Summary

Direct measurements of BrC were made on solvent extracts from filters collected at altitudes ranging from approximately 1 to 12 km over the central US during summer. The data were segregated into periods of sampling in biomass burning plumes and more typical background tropospheric conditions. The filters were extracted sequentially; first in water, then in methanol, and the sum of the water plus methanol extract BrC assumed to represent the total BrC.

During biomass burning periods, both water- and methanol-soluble BrC were highly correlated with other known emissions from biomass burning plumes, including CO, acetonitrile and BC. Under background conditions, the water-soluble fraction of BrC was somewhat correlated with smoke tracers, whereas the methanol-soluble BrC was not well correlated with any specific tracers, but most correlated with WSOC, possibly

ACPD
15, 5959–6007, 2015

due to the BrC evolving to a more water-insoluble state as it aged. BrC was 4 to 5 times higher in biomass burning plumes relative to the background conditions and more water-soluble (45 % of the total, at 365 nm, in the biomass burning plumes vs. 30 % in background air).

BrC was found throughout the tropospheric column. For background conditions, BrC was more evenly distributed throughout the column than BC, resulting in an increasing proportion of BrC relative to BC, with increasing altitude. This was consistent with an observed increasing AAE from the 3-wavelength PSAP data.

Estimates of BC and BrC absorption coefficients at 365 nm were compared to observed PSAP absorption. For background air masses, a closure between BC + BrC vs. ambient absorption coefficients derived from the PSAP resulted in a slope within 3 % of 1. For biomass burning plumes the closure was within 22 %. Reasonable closure suggests that PSAP AAEs greater than one were mainly due to the presence of BrC and not due to enhancements from BC internal mixing with other compounds, although the data do not definitely prove this.

To estimate the BrC contribution to climate forcing, the vertically-resolved data were applied to a radiative transfer model (SBDART). The overall negative TOA forcing by aerosol scattering was reduced by approximately 20 % due to BrC absorption. Thus, for the aerosol loadings recorded during this study under background conditions, BrC increased the shortwave solar absorption in the atmosphere by roughly 20 % over what would occur if it were not present. These results demonstrate that BrC is an important climate forcing agent and should be considered in global climate models.

Because there are differences in BC and BrC sources and vertical distributions, the latter has an impact on the radiative forcing (Samset and Myhre, 2011), BrC cannot be accurately represented by a simple scaling of BC. Furthermore, this study and others (Lee et al., 2014; Zhong et al., 2014) show that BrC is dynamic with significant changes possibly occurring with photochemical aging, making predicting BrC levels and optical effects of BrC complex. Instead a look-up chart was developed based on the average vertical profile for atmosphere background conditions in this study. The chart provides

ACPD
15, 5959–6007, 2015

estimates of BrC radiative forcing based on three surface-measured aerosol parameters. The look-up chart is an important first attempt at developing a tool to assess the role of BrC radiative forcing and aid in including BrC in global models. Measurements of well aged BrC vertical profiles similar to those of this study are needed in other locations to improve the predictability of this type of model.

The Supplement related to this article is available online at doi:10.5194/acpd-15-5959-2015-supplement.

Acknowledgements. This project was funded by GIT NASA contracts NNX12AB83G and NNX14AP74G and UNH NASA contract NNX12AB80G. Acetonitrile measurements onboard the DC-8 were supported by BMVIT/FFG-ALR and the NASA Postdoctoral Program. P. Campuzano-Jost, D. A. Day, and J. L. Jimenez were supported by NASA NNX12AC03G. The authors thank the DC3 personnel for logistical support.

References

Andreae, M. and Gelencser, A.: Black carbon or brown carbon? The nature of light-absorbing carbonaceous aerosols, Atmos. Chem. Phys., 6, 3131–3148, doi:10.5194/acp-6-3131-2006, 2006.

Bahadur, R., Praveen, P. S., Xu, Y. Y., and Ramanathan, V.: Solar absorption by elemental and brown carbon determined from spectral observations, P. Natl. Acad. Sci. USA, 109, 17366–17371, 2012.

Barth, M. C., Cantrell, C. A., Brune, W. H., Rutledge, S. A., Crawford, J. H., Huntrieser, H., Carey, L. D., MacGorman, D., Weisman, M., Pickering, K. E., Bruning, E., Anderson, B., Apel, E., Biggerstaff, M., Campos, T., Campuzano-Jost, P., Cohen, R., Crounse, J., Day, D. A., Diskin, G., Flocke, F., Fried, A., Garland, C., Heikes, B., Honomichl, S., Hornbrook, R., Huey, L. G., Jimenez, J. L., Lang, T., Lichtenstern, M., Mikoviny, T., Nault, B., O'Sullivan, D., Pan, L. L., Peischl, J., Pollack, I., Richter, D., Riemer, D., Ryerson, T., Schlager, H., St. Clair, J., Walega, J., Weibring, P., Weinheimer, A., Wennberg, P., Wisthaler, A.,

Wooldridge, P. J., and Ziegler, C.: The Deep Convective Clouds and Chemistry (DC3) field campaign, B. Am. Meteorol. Soc., doi:10.1175/BAMS-D-13-00290.1, in press, 2014.

Baumgardner, D., Popovicheva, O., Allan, J., Bernardoni, V., Cao, J., Cavalli, F., Cozic, J., Diapouli, E., Eleftheriadis, K., Genberg, P. J., Gonzalez, C., Gysel, M., John, A., Kirchstetter, T. W., Kuhlbusch, T. A. J., Laborde, M., Lack, D., Müller, T., Niessner, R., Petzold, A., Piazzalunga, A., Putaud, J. P., Schwarz, J., Sheridan, P., Subramanian, R., Swietlicki, E., Valli, G., Vecchi, R., and Viana, M.: Soot reference materials for instrument calibration and intercomparisons: a workshop summary with recommendations, Atmos. Meas. Tech., 5, 1869–1887, doi:10.5194/amt-5-1869-2012, 2012.

Bond, T. C. and Bergstrom, R. W.: Light absorption by carbonaceous particles: an investigative review, Aerosol Sci. Tech., 40, 27–67, 2006.

Bond, T. C., Anderson, T. L., and Campbell, D.:. Calibration and intercomparison of filter-based measurements of visible light absorption by aerosols, Aerosol Sci. Tech., 30, 582–600, 1999.

Bond, T. C., Habib, G., and Bergstrom, R. W.: Limitations in the enhancement of visible light absorption due to mixing state, J. Geophys. Res., 111, D20211, doi:10.1029/2006JD007315, 2006.

Bond, T. C., Doherty, S. J., Fahey, D. W., Forster, P. M., Berntsen, T., DeAngelo, B. J., Flanner, M. G., Ghan, S., Kärcher, B., Koch, D., Kinne, S., Kondo, Y., Quinn, P. K., Sarofim, M. C., Schultz, M. G., Schulz, M., Venkataraman, C., Zhang, H., Zhang, S., Bellouin, N., Guttikunda, S. K., Hopke, P. K., Jacobson, M. Z., Kaiser, J. W., Klimont, Z., Lohmann, U., Schwarz, J. P., Shindell, D., Storelvmo, T., Warren, S. G., and Zender C. S.: Bounding the role of black carbon in the climate system: a scientific assessment, J. Geophys. Res. Atmos., 118, 5380–5552: doi:10.1002/jgrd.50171, 2013.

Bush, B. and Valero, F. P. J.: Surface aerosol radiative forcing at Gosan during the ACE-Asia campaign, J. Geophys. Res., 108, 8660, doi:10.1029/2002JD003233, 2003.

Cappa, C. D., Onasch, T. B., Massoli, P., Worsnop, D. R., Bates,T. S., Cross, E. S., Davidovits, P., Hakala, J., Hayden, K. L., Jobson, B. T., Kolesar, K. R., Lack, D. A., Lerner, B. M., Li, S. M., Mellon, D., Nuaaman, I., Olfert, J. S., Petaja, T., Quinn, P. K., Song, C., Subramanian, R., Williams, E. J., and Zaveri, R. A.: Radiative absorption enhancements due to the mixing state of atmospheric black carbon, Science, 337, 1078–1081, 2012.

Carrico, C. M., Bergin, M. H., Xu, J., Baumann, K., and Maring, H.: Urban aerosol radiative properties: measurements during the 1999 Atlanta supersite experiment, J. Geophys. Res.-Atmos., 108, 8422, doi:10.1029/2001JD001222, 2003.

ACPD
15, 5959–6007, 2015

Chan, T. W., Brook, J. R., Smallwood, G. J., and Lu, G.: Time-resolved measurements of black carbon light absorption enhancement in urban and near-urban locations of southern Ontario, Canada, Atmos. Chem. Phys., 11, 10407–10432, doi:10.5194/acp-11-10407-2011, 2011.

Chen, Y. and Bond, T. C.: Light absorption by organic carbon from wood combustion, Atmos. Chem. Phys., 10, 1773–1787, doi:10.5194/acp-10-1773-2010, 2010.

Chung, C. E., Ramanathan, V., and Decremer, D.: Observationally constrained estimates of carbonaceous aerosol radiative forcing, P. Natl. Acad. Sci. USA, 109, 11624–11629, 2012.

Clarke, A., McNaughton, C., Kapustin, V., Shinozuka, Y., Howell, S., Dibb, J., Zhou, J., Anderson, B., Brekhovskikh, V., Turner, H., and Pinkerton, M.: Biomass burning and pollution aerosol over North America: organic components and their influence on spectral optical properties and humidification response, J. Geophys. Res., 112, D12S18, doi:10.1029/2006JD007777, 2007.

DeCarlo, P. F., Kimmel, J. R., Trimborn, A., Northway, M. J., Jayne, J. T., Aiken, A. C., Gonin, M., Fuhrer, K., Horvath, T., Docherty, K. S., Worsnop, D. R., and Jimenez, J. L.: Field-deployable, high-resolution, time-of-flight aerosol mass spectrometer, Anal. Chem., 78, 8281–8289, 2006.

de Gouw, J. A., Cooper, O. R., Warneke, C., Hudson, P. K., Fehsenfeld, F. C., Holloway, J. S., Hübler, G., Nicks Jr., D. K., Nowak, J. B., Parrish, D. D., Ryerson, T. B., Atlas, E. L., Donnelly, S. G., Schauffler, S. M., Stroud, V., Johnson, K., Carmichael, G. R., and Streets, D. G.:. Chemical composition of air masses transported from Asia to the US West Coast during ITCT 2K2: fossil fuel combustion vs. biomass-burning signatures, J. Geophys. Res., 109, D23S20, doi:10.1029/2003JD004202, 2004.

de Haan, D. O., Corrigan, A. L., Smith, K. W., Stroik, D. R., Turley, J. J., Lee, F. E., Tolbert, M. A., Jimenez, J. L., Cordova, K. E., and Ferrell, G. R.: Secondary organic aerosol-forming reactions of glyoxal with amino acids, Environ. Sci. Techol., 43, 2818–2824, 2009.

Desyaterik, Y., Sun, Y., Shen, X., Lee, T., Wang, X., Wang, T., and Collett Jr., J. L.: Speciation of “brown” carbon in cloud water impacted by agricultural biomass burning in eastern China, J. Geophys. Res.-Atmos., 118, 7389–7399, doi:10.1002/jgrd.50561, 2013.

Feng, Y., Ramanathan, V., and Kotamarthi, V. R.: Brown carbon: a significant atmospheric absorber of solar radiation?, Atmos. Chem. Phys., 13, 8607–8621, doi:10.5194/acp-13-8607-2013, 2013.

Gyawali, M., Arnott, W. P., Lewis, K., and Moosmüller, H.: In situ aerosol optics in Reno, NV, USA during and after the summer 2008 California wildfires and the influence of absorbing

and non-absorbing organic coatings on spectral light absorption, Atmos. Chem. Phys., 9, 8007–8015, doi:10.5194/acp-9-8007-2009, 2009.

Hecobian, A., Zhang, X., Zheng, M., Frank, N., Edgerton, E. S., and Weber, R. J.: Water-Soluble Organic Aerosol material and the light-absorption characteristics of aqueous extracts measured over the Southeastern United States, Atmos. Chem. Phys., 10, 5965–5977, doi:10.5194/acp-10-5965-2010, 2010.

Hoffer, A., Gelencsér, A., Guyon, P., Kiss, G., Schmid, O., Frank, G. P., Artaxo, P., and Andreae, M. O.: Optical properties of humic-like substances (HULIS) in biomass-burning aerosols, Atmos. Chem. Phys., 6, 3563–3570, doi:10.5194/acp-6-3563-2006, 2006.

IPCC: Climate Change: The Physical Science Basis, Contribution of Working Group I to the UN IPCC's 5th Assessment Report, Cambridge University Press, New York (USA), 2013.

Kieber, R. J., Whitehead, R. F., Reid, S. N., Willey, J. D., and Seaton, P. J.: Chromophoric dissolved organic matter (CDOM) in rainwater, southeastern North Carolina, USA, J. Atmos. Chem., 54, 21–41, 2006.

Kirchstetter, T. W., Novakov, T., and Hobbs, P. V.: Evidence that the spectral dependence of light absorption by aerosols is affected by organic carbon, J. Geophys. Res., 109, D21208, doi:10.1029/2004JD004999, 2004.

Kirchstetter, T. W. and Thatcher, T. L.: Contribution of organic carbon to wood smoke particulate matter absorption of solar radiation, Atmos. Chem. Phys., 12, 5803–5816, doi:10.5194/acpd-12-5803-2012. 2012.

Koch, D., Bond, T. C., Streets, D., Unger, N., and van der Werf, G. R.: Global impacts of aerosols from particular source regions and sectors, J. Geophys. Res., 112, D02205: doi:10.1029/2005JD007024, 2007.

Lack, D. A. and Cappa, C. D.: Impact of brown and clear carbon on light absorption enhancement, single scatter albedo and absorption wavelength dependence of black carbon, Atmos. Chem. Phys., 10, 4207–4220, doi:10.5194/acp-10-4207-2010, 2010.

Lack, D. A. and Langridge, J. M.: On the attribution of black and brown carbon light absorption using the Ångström exponent, Atmos. Chem. Phys., 13, 10535–10543, doi:10.5194/acp-13-10535-2013, 2013.

Lack, D. A., Cappa, C. D., Covert, D. S., Baynard, T., Massoli, P., Sierau, B., Bates, T. S., Quinn, P. K., Lovejoy, E. R., and Ravishankara, A. R.: Bias in filter-based aerosol light absorption measurements due to organic aerosol loading: evidence from ambient measurements, Aerosol Sci. Tech., 42, 1033–1041, 2008.

Lack, D. A., Bahreini, R., Langridge, J. M., Gilman, J. B., and Middlebrook, A. M.: Brown carbon absorption linked to organic mass tracers in biomass burning particles, Atmos. Chem. Phys., 13, 2415–2422, doi:10.5194/acp-13-2415-2013, 2013.

Lee, H. J., Aiona, P. K., Laskin, A., Laskin, J., and Nizkorodov, S. A.: Effect of solar radiation on the optical properties and molecular composition of laboratory proxies of atmospheric brown carbon, Environ. Sci. Technol., 48, 10217–10226, 2014.

Limbeck, A., Kulmala, M., and Puxbaum, H.: Secondary organic aerosol formation in the atmosphere via heterogeneous reaction of gaseous isoprene on acidic particles, Geophys. Res. Lett., 30, doi:10.1029/2003GL017738, 2003.

Liu, J., Scheuer, E., Dibb, J. E., Ziemba, L. D., Thornhill, K. L., Anderson, B. E., Wisthaler, A., Mikoviny, T., Devi, J. J., Bergin, M., and Weber, R. J.: Brown cabon in the continential troposphere, Geophys. Res. Lett., 41, 2191–2195, doi:10.1002/2013GL058976, 2014.

Liu, J., Bergin, M., Guo, H., King, L., Kotra, N., Edgerton, E., and Weber, R. J.: Size-resolved measurements of brown carbon in water and methanol extracts and estimates of their contribution to ambient fine-particle light absorption, Atmos. Chem. Phys., 13, 12389–12404, doi:10.5194/acp-13-12389-2013, 2013.

Lukacs, H., Gelencser, A., Hammer, S., Puxbaum, H., Pio, C., Legrand, M., Kasper-Giebl, A., Handler, M., Limbeck, A., Simpson, D., and Preunkert, S.: Seasonal trends and possible sources of brown carbon based on 2 year aerosol measurements at six sites in Europe, J. Geophys. Res., 112, D23S18 doi:10.1029/2006JD008151, 2007.

McNaughton, C. S., Clarke, A. D., Howell, S. G., Pinkerton, M., Anderson, B., Thornhill, L., Hudgins, C., Winstead, E., Dibb, J. E., Scheuer, E., and Maring, H.: Results from the DC-8 inlet characterization experiment (DICE): airborne vs. surface sampling of mineral dust and sea salt aerosols, Aerosol Sci. Tech., 41, 136–159, 2007.

Mohr, C., Lopez-Hilfiker, F. D., Zotter, P., Prévôt, A. S. H., Xu, L., Ng, N. L., Herndon, S. C., Williams, L. R., Franklin, J. P., Zahniser, M. S., Worsnop, D. R., Knighton, W. B., Aiken, A. C., Gorkowski, K. J., Dubey, M. K., Allan, J. D., Thornton, J. A.: Contribution of nitrated phenols to wood burning brown carbon light absorption in Detling, UK during winter time, Environ. Sci. Technol., 47, 6316–6324, doi:10.1021/es400683v, 2013.

Moosmüller, H., Chakrabarty, R. K., Ehlers, K. M., and Arnott, W. P.: Absorption Ångström coefficient, brown carbon, and aerosols: basic concepts, bulk matter, and spherical particles, Atmos. Chem. Phys., 11, 1217–1225, doi:10.5194/acp-11-1217-2011, 2011.

Myhre, G., Hoyle, C. R., Berglen, T. F., Johnson, B. T., and Haywood, J. M.: Modeling of the solar radiative impact of biomass burning aerosols during the Dust and Biomass-burning Experiment (DABEX), J. Geophys. Res., 113, D00C16, doi:10.1029/2008JD009857, 2008.

Park, R. J., Kim, M. J., Jeong, J. I., Yooun, D., and Kim, S.: A contribution of brown carbon aerosol to the aerosol light absorption and its radiative forcing in East Asia, Atmos. Environ., 44, 1414–1421, 2010.

Petzold, A., Schloesser, H., Sheridan, P. J., Arnott, W. P., Ogren, J. A., and Virkkula, A.: Evaluation of multi-angle absorption photometry for measuring aerosol light absorption, Aerosol Sci. Tech., 39, 40–51, 2005.

Saleh, R., Hennigan, C. J., McMeeking, G. R., Chuang, W. K., Robinson, E. S., Coe, H., Donahue, N. M., and Robinson, A. L.: Absorptivity of brown carbon in fresh and photo-chemically aged biomass-burning emissions, Atmos. Chem. Phys., 13, 7683–7693, doi:10.5194/acp-13-7683-2013, 2013.

Samset, B. H. and Myhre, G.: Vertical dependence of black carbon, sulphate and biomass burning aerosol radiative forcing, Geophys. Res. Lett., 38, L24802, doi:10.1029/2011GL049697, 2011.

Sandradewi, J., Prévôt, A. S. H., Alfarra, M. R., Szidat, S., Wehrli, M. N., Ruff, M., Weimer, S., Lanz, V. A., Weingartner, E., Perron, N., Caseiro, A., Kasper-Giebl, A., Puxbaum, H., Wacker, L., and Baltensperger, U.: Comparison of several wood smoke markers and source apportionment methods for wood burning particulate mass, Atmos. Chem. Phys. Discuss., 8, 8091–8118, doi:10.5194/acpd-8-8091-2008, 2008.

Sareen, N., Schwier, A. N., Shapiro, E. L., Mitroo, D., and McNeill, V. F.: Secondary organic material formed by methylglyoxal in aqueous aerosol mimics, Atmos. Chem. Phys., 10, 997–1016, doi:10.5194/acp-10-997-2010, 2010.

Schnaiter, M., Schmid, O., Petzold, A., Fritzsche, L., Klein, K. F., Andreae, M. O., Helas, G., Thielmann, A., Gimmler, M., Mohler, O. M., Linke, C., and Schurath, U.: Measurement of wavelength resolved light absorption by aerosols utilizing a UV-VIS extinction cell, Aerosol Sci. Tech., 39, 249–260, 2005.

Schwarz, J. P., Spackman, J. R., Fahey, D. W., Gao, R. S., Lohmann, U., Stier, P., Watts, L. A., Thomson, D. S., Lack, D. A., Pfister, L., Mahoney, M. J., Baumgardner, D., Wilson, J. C., and Reeves, J. M.: Coatings and their enhancement of black carbon light absorption in the tropical atmosphere, J. Geophys. Res., 113, D03203, doi:10.1029/2007JD009042, 2008.

ACPD
15, 5959–6007, 2015

Slowik, J. G., Cross, E. S., Han, J. H., Davidovits, P., Onasch, T. B., Jayne, J. T., Williams, L. R., Canagaratna, M. R., Worsnop, D. R., Chakrabarty, R. K., Moosmüller, H., Arnott, W. P., Schwarz, J. P., Gao, R. S., Fahey, D. W., Kok, G. L., and Petzold, A.: An inter-comparison of instruments measuring black carbon content of soot particles, Aerosol Sci. Tech., 41, 295–314, doi:10.1080/02786820701197078, 2007.

Sun, H. L., Biedermann, L., and Bond, T. C.: Color of brown carbon: a model for ultraviolet and visible light absorption by organic carbon aerosol, Geophys. Res. Lett., 34, L17813, doi:10.1029/2007GL029797, 2007.

Virkkula, A.: Correction of the calibration of the 3-wavelength particle soot absorption photometer (3 PSAP), Aerosol Sci. Tech. 44, 706–712, 2010.

Washenfelder, R. A., Attwood, A. R., Brock, C. A., Guo, H., Xu, L., Weber, R. J., Ng, N. L., Allen, H. M., Ayres, W. R., Baumann, K., Cohen, R. C., Draper, D. C., Duffey, K. C., Edgerton, E., Fry, J. L., Hu, W. W., Jimenez, J. L., Palm, B. B., Romer, P., Stone, E. A., Wooldridge, P. J., and Brown, S. S.: Biomass burning dominates brown carbon absorption in the rural southeastern United States, Geophys. Res. Lett., 42, 653–664, doi:10.1002/2014GL062444, 2015.

Yang, M., Howell, S. G., Zhuang, J., and Huebert, B. J.: Attribution of aerosol light absorption to black carbon, brown carbon, and dust in China – interpretations of atmospheric measurements during EAST-AIRE, Atmos. Chem. Phys., 9, 2035–2050, doi:10.5194/acp-9-2035-2009, 2009.

Zarzana, K. J., Haan, D. O. D., Freedman, M. A., Hasenkopf, C. A., and Tolbert, M. A.: Optical properties of the products of α-dicarbonyl and amine reactions in simulated cloud droplets, Environ. Sci. Technol., 46, 4845–4851, 2012.

Zhang, X. L., Liu, J. M., Parker, E. T., Hayes, P. L., Jimenez, J. L., de Gouw, J. A., Flynn, J. H., Grossberg, N., Lefer, B. L., and Weber, R. J.: On the gas-particle partitioning of soluble organic aerosol in two urban atmospheres with contrasting emissions, 1, bulk water-soluble organic carbon, J. Geophys. Res.-Atmos., 117, D00V16, doi:10.1029/2012JD017908, 2012.

Zhang, X., Lin, Y.-H., Surratt, J. D., and Weber, R. J.: Sources, composition and absorption Angström exponent of light-absorbing organic components in aerosol extracts from the Los Angeles Basin, Environ. Sci. Technol., 47, 3685–3693, 2013.

Zhang, X., Lin, Y.-H., Surratt, J. D., Zotter, P., Prevot, A. S. H., and Weber, R. J.: Light-absorbing soluble organic aerosol in Los Angeles and Atlanta: a contrast in secondary organic aerosol, Geophys. Res. Lett., 38, L21810: doi:10.1029/2011GL049385, 2011.

ACPD
15, 5959–6007, 2015

Zhong, M. and Jang, M.: Dynamic light absorption of biomass-burning organic carbon photochemically aged under natural sunlight, Atmos. Chem. Phys., 14, 1517–1525, doi:10.5194/acp-14-1517-2014, 2014.

ACPD
15, 5959–6007, 2015

Table 1. Nomenclature.

PSAP	Particle Soot Absorption Photometer
b_{ap}	light absorption coefficient for fine particles (M/m)
BC	Black Carbon
BrC	Brown Carbon
WSOC	Water-Soluble Organic Carbon ($\mu g\,C/m^3$)
OA	Organic Aerosol ($\mu g\,m^{-3}$)
AAE	Absorption Ångström Exponent
AAE_{BrC}	Absorption Ångström Exponent for brown carbon from solution data
AAE_{BC}	Absorption Ångström Exponent for black carbon
AAE_{PSAP}	Absorption Ångström Exponent based on the PSAP data
$A(\lambda)$	light absorbance measured by the spectrophotometer, (unitless)
$Abs(\lambda)$	light absorption measured in a solution at wavelength λ (M/m)
$H_2O\_Abs(\lambda)$	light absorption measured in water-extract at wavelength λ (M/m)
$MeOH\_Abs(\lambda)$	light absorption measured in methanol-extract at wavelength λ (M/m)
$Total\_Abs(\lambda)$	sum of $H_2O\_Abs(\lambda)$ and $MeOH\_Abs(\lambda)$ for a filter extracted sequentially using the two solvents (water then methanol).
$b_{ap,H_2O\_BrC}(\lambda)$	Mie predicted fine particle brown carbon absorption from water extracts (M/m), wavelength is specified in text.
$b_{ap,Total\_BrC}(\lambda)$	Mie predicted fine particle brown carbon absorption from the sum of water and methanol extracts (M/m), wavelength is specified in text.
$b_{ap,PSAP}(\lambda)$	Light absorption coefficient of fine particles at wavelength λ (M/m) determined from the PSAP data.
$b_{ap,BC1}(\lambda)$	Light absorption coefficient of BC at wavelength λ (M/m), estimated from PSAP absorption at 660 nm, assuming non-BC light absorbers are minimal at 660 nm and an AAE_{BC} of 1
$b_{ap,BC2}(\lambda)$	Light absorption coefficient of BC at wavelength λ (M/m), estimated using a mass absorption cross section of $7.5\,m^2\,g^{-1}$ at 550 nm and an AAE_{BC} of 1
$b_{ap2}(\lambda)$	Light absorption coefficient of fine particles at wavelength λ (M/m) determined from $b_{ap,BC2}(660)$ and AAE_{PSAP}
MAC	Mass Absorption Cross-section
SZA	Solar Zenith Angle
TOA	Top of Atmosphere
a.s.l.	Above sea level
SD	Standard Deviation

ACPD
15, 5959–6007, 2015

Table 2. Periods of identified biomass-burning plumes.

Time (UTC)
25 May 2012, 22:00–22:26
26 May 2012, 21:20–21:40, 27 May 2012, 00:09–00:21
6 June 2012, 21:27–21:37, 7 June 2012, 00:19–00:36
11 June 2012 16:24–16:57, 17:56–18:11, 21:56–22:06
15 June 2012, 19:51–20:10
16 June 2012, 21:18–21:26, 17 June 2012 01:36–02:13
17 June 2012, whole flight
22 June 2012, whole flight

ACPD
15, 5959–6007, 2015

Table 3. Statistical summary of observed species throughout all flights during DC3 separated into three categories: all samples, samples during identified biomass burning events and samples for background conditions (periods when data could not be clearly identified as biomass burning). For statistical purposes, 1/2 the LOD value is substituted for data below LOD. All data have been merged to the nominally 5 min filter sampling time.

	LOD	% above LOD	Mean	Median	Std Dev	Min	Max
All samples							
WSOC[a]	0.084	95	1.24	0.81	1.83	0.042	31.37
OA[b]	0.30	89	3.48	2.82	10.85	0.15	208.53
BC[b]	0.01	84	0.069	0.036	0.189	0.005	3.75
H_2O_Abs(365)[c]	0.031	87	0.33	0.11	1.93	0.016	39.50
Total_Abs(365)[c]	0.11	86	0.94	0.44	3.89	0.055	67.19
Biomass Burning events							
WSOC	0.084	94	1.52	0.77	3.93	0.042	31.37
OA	0.30	88	7.55	3.73	25.95	0.15	208.53
BC	0.01	83	0.144	0.052	0.47	0.005	3.75
H_2O_Abs(365)	0.031	92	1.03	0.32	4.66	0.016	39.50
Total_Abs(365)	0.11	93	2.37	0.86	8.67	0.055	67.19
Background conditions							
WSOC	0.084	95	1.19	0.82	1.28	0.042	10.68
OA	0.30	93	2.69	2.01	2.69	0.15	12.79
BC	0.01	88	0.056	0.035	0.060	0.005	0.399
H_2O_Abs(365)	0.031	86	0.20	0.10	0.53	0.016	7.52
Total_Abs(365)	0.11	85	0.64	0.36	1.38	0.055	15.44

[a] unit: $\mu gC/m^3$;
[b] unit: $\mu g/m^3$;
[c] unit: Mm^{-1}

ACPD
15, 5959–6007, 2015

Table 4. Pearson rank correlations (r) for biomass burning plumes and background conditions. Bold values above the matrix diagonal are from biomass burning plumes (69 data points), while italic numbers below the matrix diagonal are from background conditions (334 data points). All data were averaged to filter sampling times.

	WSOC	H_2O_Abs(365)	Total_Abs(365)	OA	CO	BC	Acetonitrile	$b_{ap,PSAP}(470)$	$b_{ap,PSAP}(532)$	$b_{ap,PSAP}(660)$
WSOC	1	**0.99**	**0.97**	**0.96**	**0.93**	**0.70**	**0.97**	**0.75**	**0.75**	**0.75**
H_2O_Abs(365)	0.34	1	**0.98**	**0.98**	**0.94**	**0.72**	**0.98**	**0.7**	**0.78**	**0.78**
Total_Abs(365)	0.13	0.32	1	**0.995**	**0.97**	**0.83**	**0.99**	**0.87**	**0.87**	**0.87**
OA	0.28	0.57	0.20	1	**0.97**	**0.85**	**0.99**	**0.89**	**0.89**	**0.89**
CO	0.15	0.48	0.17	0.76	1	**0.85**	**0.97**	**0.87**	**0.87**	**0.87**
BC	0.20	0.64	0.30	0.86	0.75	1	**0.82**	**0.99**	**0.99**	**0.99**
Acetonitrile	0.11	0.57	0.23	0.48	0.52	0.57	1	**0.86**	**0.86**	**0.86**
$b_{ap,PSAP}(470)$	0.27	0.66	0.31	0.80	0.72	0.95	0.58	1	**0.9999**	**0.9997**
$b_{ap,PSAP}(532)$	0.27	0.63	0.31	0.80	0.72	0.95	0.55	0.99	1	**0.9999**
$b_{ap,PSAP}(660)$	0.28	0.59	0.29	0.80	0.70	0.93	0.51	0.98	0.99	1

ACPD
15, 5959–6007, 2015

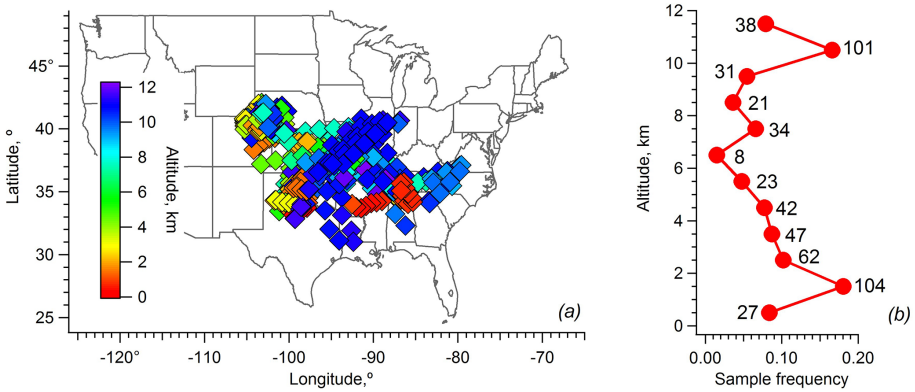

Figure 1. (a) Filter collection sampling locations, color-coded by altitude, and **(b)** sampling frequency vs. altitude for the complete DC3 mission, with number of filters for each altitude bin given.

ACPD
15, 5959–6007, 2015

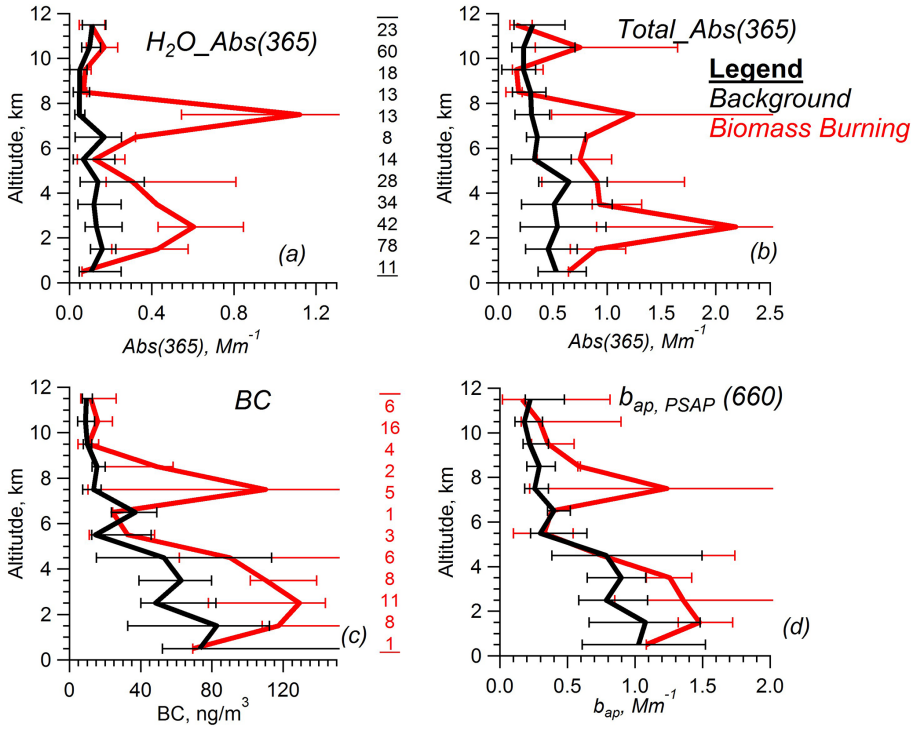

Figure 2. Vertical profiles of absorption measured in filter water extracts and the sum of water and methanol extract (total), both at 365 nm, SP2 BC concentration, and PSAP absorption at 660 nm. Data are binned into 1 km ranges and the median values are shown. Error bars indicate inter-quartile ranges. The column in the middle shows the number of data points in each altitude bin, with black for background conditions (upper) and red for biomass burning (bottom row).

ACPD
15, 5959–6007, 2015

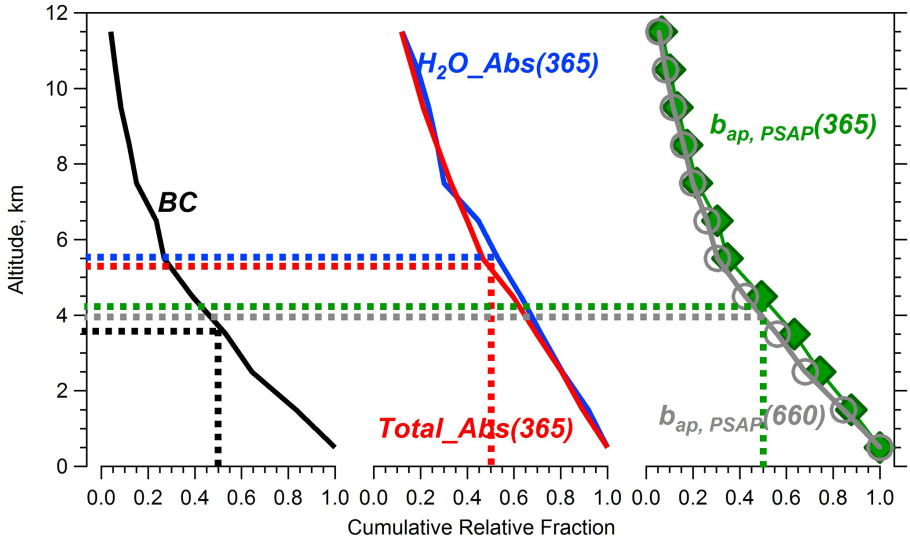

Figure 3. Vertical profile of the relative cumulative fraction (summed over all altitudes above vs. the total column), for BC (SP2), brown carbon at 365 nm based on extract solution absorption, PSAP absorption at 660 nm, and estimated PSAP total aerosol absorption at 365 nm, during background tropospheric conditions.

ACPD
15, 5959–6007, 2015

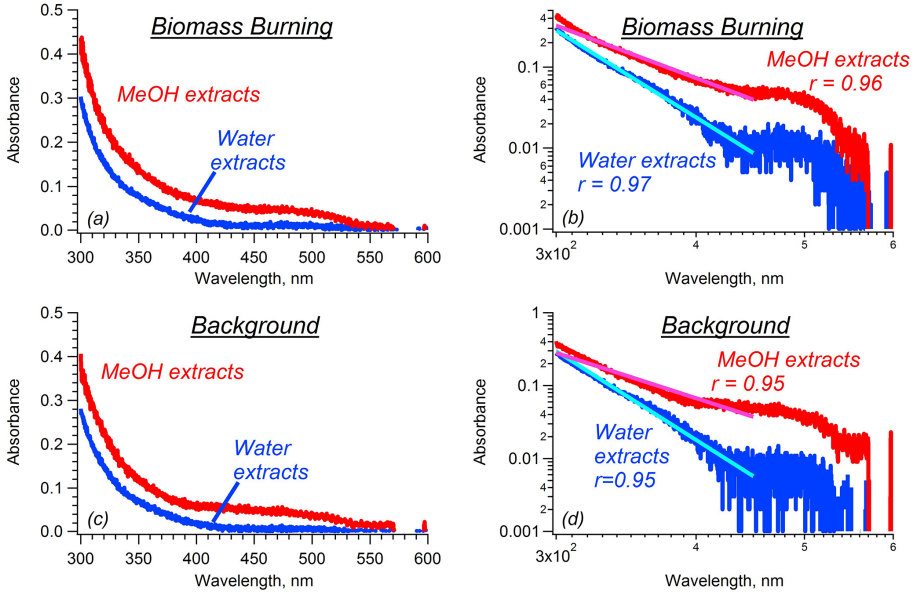

Figure 4. Example solution spectra of H_2O and MeOH (methanol) extracts for biomass burning as well as background tropospheric conditions. Absorption Ångström exponent is calculated by a linear regression fit to log Abs vs. log λ in the wavelength range of 300–450 nm, with an average r value of 0.87 for water extracts, and 0.84 for methanol extracts for background data, and larger than 0.9 r value for biomass burning filter extracts, for both water and methanol.

ACPD
15, 5959–6007, 2015

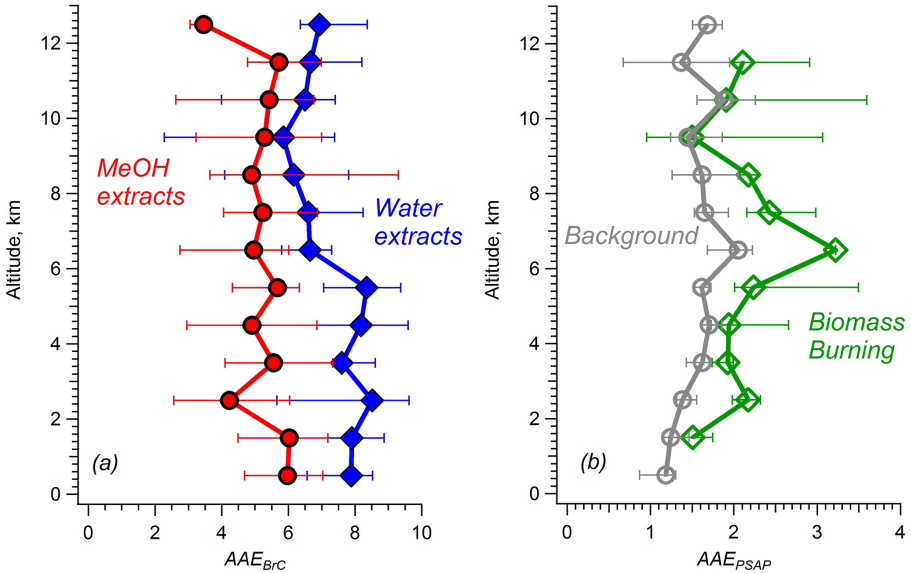

Figure 5. Vertical profiles of Absorption Ångström Exponent (AAE) of **(a)** brown carbon from solution spectra of both water extracts (blue line) and methanol extracts (red line), for background conditions, and **(b)** PSAP absorption measurements based on the wavelength combination (470, 660 nm), both background and biomass burning impacted periods. Data were binned by 1 km increments. Error bars indicated the inter-quartile range.

ACPD
15, 5959–6007, 2015

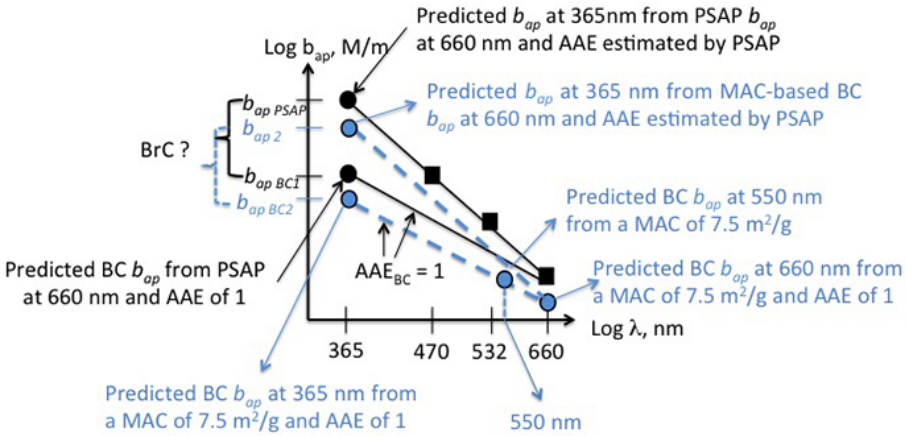

Figure 6. Schematic of how ambient aerosol and BC absorption was extrapolated to lower wavelengths. Square data points represent PSAP measurement, which are used to estimate the ambient aerosol AAE (AAE_{PSAP}, not shown but slope of upper lines), and used to predict ambient aerosol absorption at 365 nm ($b_{ap,PSAP}$). Light absorption by black carbon ($b_{ap,BC}$) is estimated assuming an AAE_{BC} of 1 and extrapolating from the PSAP measurement at 660 nm, a size where BrC absorption is minimal, or alternatively assuming a BC MAC of 7.5 $m^2\,g^{-1}$ at 550 nm and extrapolating to 365 nm with an AAE_{BC} of 1.

ACPD
15, 5959–6007, 2015

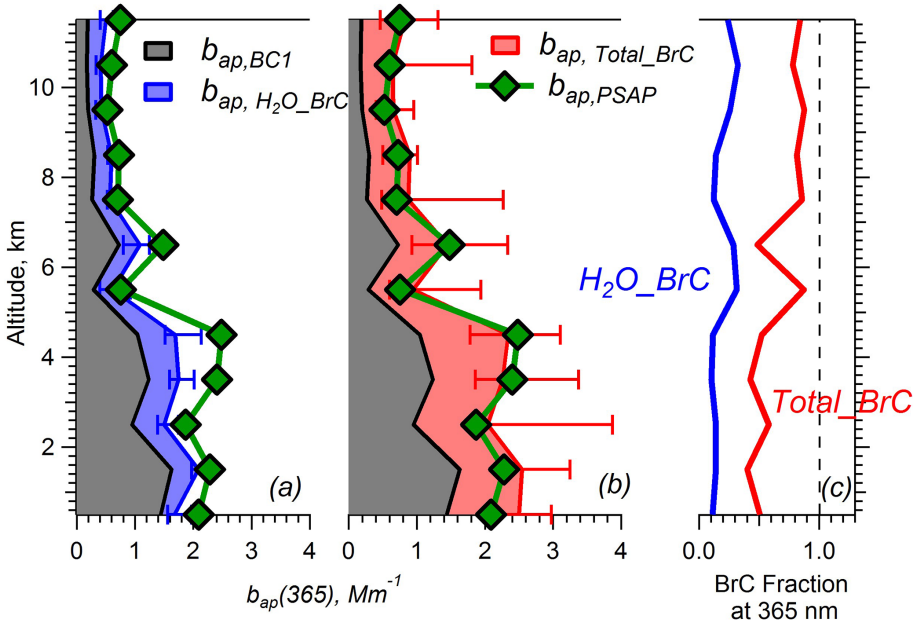

Figure 7. Vertical profiles of estimated aerosol optical absorption at 365 nm by BrC, BC, determined by an extrapolation from PSAP absorption at 660 nm ($b_{ap,BC1}$ shown in the schematic), and the sum of BrC and BC compared to total light-absorbing determined from the PSAP data. Figure **(a)** shows water-soluble BrC (blue shaded), **(b)** the total BrC (red shaded) and **(c)** relative contribution of BrC to total aerosol absorption. In all plots, median values are shown and error bars indicate the inter-quartile range of estimated BrC absorption for each 1 km altitude bin. (Measurement uncertainties of the various absorption coefficients are estimated to be between ±28 and ±45 %). Only background tropospheric data are plotted.

ACPD
15, 5959–6007, 2015

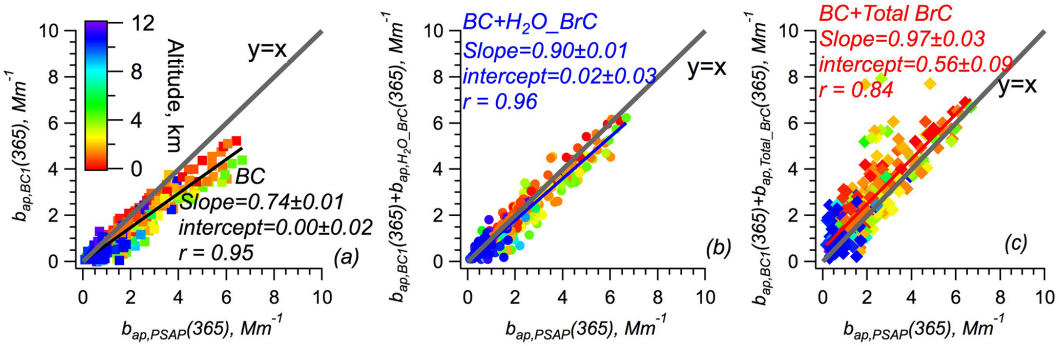

Figure 8. Closure analysis of b_{ap} at 365 nm for background tropospheric conditions. Scatter plots of estimated **(a)** BC absorption, and **(b)** sum of BC absorption and water-soluble BrC absorption, and **(c)** sum of BC absorption and Total BrC absorption, compared with total aerosol absorption estimated by PSAP. Markers are color-coded by altitude. Orthogonal distance regression (ODR) fit results are shown. The 1 : 1 line is also included. (Measurement uncertainties of the various absorption coefficients are estimated to be between ±28 and ±45 %).

ACPD
15, 5959–6007, 2015

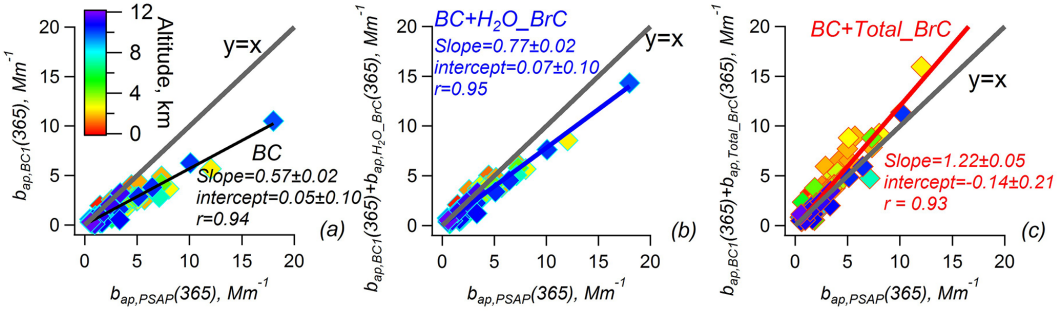

Figure 9. Closure analysis of b_{ap} at 365 nm for biomass burning plumes via scatter plots of estimated **(a)** BC absorption, and **(b)** sum of BC absorption and water-soluble BrC absorption, and **(c)** sum of BC absorption and Total BrC absorption compared with total aerosol absorption based on PSAP data. Markers were color-coded by altitude. Orthogonal distance regression (ODR) fit results are shown. The 1 : 1 line is also included. (Measurement uncertainties of the various absorption coefficients are estimated to be between ±28 and ±45 %).

ACPD
15, 5959–6007, 2015

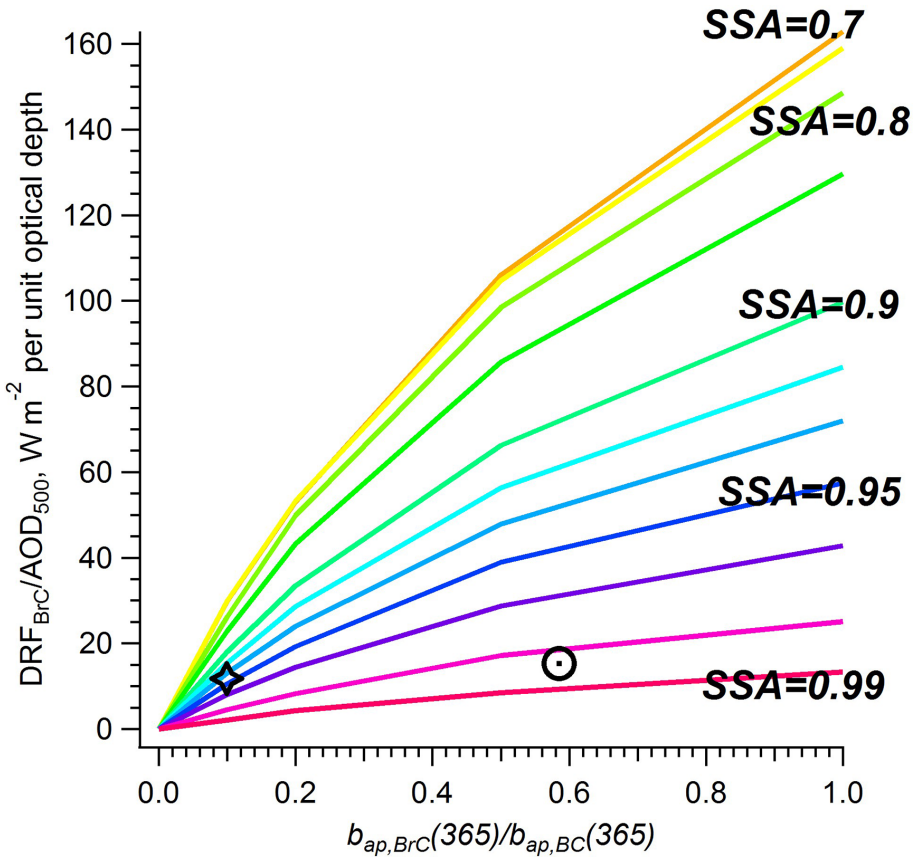

Figure 10. BrC radiative forcing efficiencies, defined as the BrC TOA direct radiative forcing divided by AOD at 500 nm, as a function of BrC to BC absorption ratio and SSA measured at surface at 365 nm. The circle corresponds to average background conditions determined from the DC3 campaign. The star represents a surface measurement from southeast US, where altitude-resolved data were not available.

ACPD
15, 5959–6007, 2015